Original Article

MOLECULAR METABOLISM

Comprehensive and quantitative analysis of white and brown adipose tissue by shotgun lipidomics

Michal Grzybek [1,2,6], Alessandra Palladini [1,2,6], Vasileia I. Alexaki [3], Michal A. Surma [4,5], Kai Simons [4], Triantafyllos Chavakis [1,2,3], Christian Klose [4,], Ünal Coskun [1,2,*,7]**

ABSTRACT

Objective: Shotgun lipidomics enables an extensive analysis of lipids from tissues and fluids. Each specimen requires appropriate extraction and processing procedures to ensure good coverage and reproducible quantification of the lipidome. Adipose tissue (AT) has become a research focus with regard to its involvement in obesity-related pathologies. However, the quantification of the AT lipidome is particularly challenging due to the predominance of triacylglycerides, which elicit high ion suppression of the remaining lipid classes.

Methods: We present a new and validated method for shotgun lipidomics of AT, which tailors the lipid extraction procedure to the target specimen and features high reproducibility with a linear dynamic range of at least 4 orders of magnitude for all lipid classes.

Results: Utilizing this method, we observed tissue-specific and diet-related differences in three AT types (brown, gonadal, inguinal subcutaneous) from lean and obese mice. Brown AT exhibited a distinct lipidomic profile with the greatest lipid class diversity and responded to high-fat diet by altering its lipid composition, which shifted towards that of white AT. Moreover, diet-induced obesity promoted an overall remodeling of the lipidome, where all three AT types featured a significant increase in longer and more unsaturated triacylglyceride and phospholipid species.

Conclusions: The here presented method facilitates reproducible systematic lipidomic profiling of AT and could be integrated with further —omics approaches used in (pre-) clinical research, in order to advance the understanding of the molecular metabolic dynamics involved in the pathogenesis of obesity-associated disorders.

Keywords Shotgun mass spectrometry; Lipidomics; Adipose tissue; Method validation; Lipid extraction; Mouse; Chow and high-fat diet; Lipid remodeling

1. INTRODUCTION

Adipose tissue (AT) in mammals plays a critical role in systemic energy homeostasis [1—3]. Two main AT forms exist, white adipose tissue (WAT), which functions primarily as an energy reservoir, and brown adipose tissue (BAT), which contributes to thermoregulation, i.e. the production of heat to maintain body temperature stability during cold exposure through non-shivering thermogenesis. The expansion of AT observed in obesity is accompanied by local hypoxia [4—6], low-grade inflammation [7—11], development of systemic insulin resistance [5], and alterations in the secretion of fatty acids [12] or adipokines [4]. Thus, studying the regulation of lipid flux and metabolism in AT and changes thereof linked to obesity is important for understanding the central role of AT in obesity-related metabolic dysfunction.

Quantitative lipid analysis of biological samples by direct infusion mass spectrometry has proven to be a powerful tool for studying lipid metabolism [13—18]. It requires comparatively low sample amounts (e.g. 1 μl of plasma is sufficient to quantify a lipidome with comprehensive coverage [19]), relatively short measurement times - a prerequisite for the high-throughput analysis of large sample numbers, and exhibits excellent technical reproducibility. The use of internal standards enables direct quantification and application to a wide range of sample types, such as yeast [13,16] flies [20], *C. elegans* [21], cellular samples [14,17,18] or various tissue and body fluids [19]. With regards to lipid quantification, ATs are particularly challenging because

[1]Paul Langerhans Institute Dresden of the Helmholtz Zentrum Munich at the University Clinic Carl Gustav Carus, TU Dresden, Dresden, Germany [2]German Center for Diabetes Research (DZD e.V.), Neuherberg, Germany [3]Institute for Clinical Chemistry and Laboratory Medicine, Faculty of Medicine, TU Dresden, Dresden, Germany [4]Lipotype GmbH, Dresden, Germany

[5] Present affiliation- PORT Sp. z o.o., Wroclaw, Poland.
[6] Michal Grzybek and Alessandra Palladini contributed equal to this work.
[7] Lead contact coskun@plid.de

*Corresponding author. Paul Langerhans Institute Dresden of the Helmholtz Zentrum Munich at the University Clinic Carl Gustav Carus, TU Dresden, Dresden, Germany. E-mail: coskun@plid.de (Ü. Coskun).

**Corresponding author. E-mail: klose@lipotype.de (C. Klose).

Received November 15, 2018 • Revision received January 17, 2019 • Accepted January 23, 2019 • Available online 30 January 2019

https://doi.org/10.1016/j.molmet.2019.01.009

of their high content of neutral lipids (>99% triacylglycerols and cholesterol esters) that causes high ion suppression of the less abundant membrane lipids [9,22–24]. Previous approaches towards AT lipidomics analysis reported differences between BAT and WAT and demonstrated remodeling upon exercise or cold exposure. However, these studies applied generic methods of lipid extraction and measurement rather than techniques tailored to these tissues [23–26].

Here we present a shotgun lipidomics method for the analysis for ATs with an unprecedented coverage of more than 300 lipid species encompassing 20 lipid classes, and featuring high reproducibility with a linear dynamic range of at least 4 orders of magnitude for all lipid classes. We not only observe clear differences between BAT and WAT lipidomes, but also amongst WAT subtypes, i.e. gonadal (GAT) and inguinal subcutaneous (SAT) ATs. Furthermore, our protocol allows for assessing the impact of high-fat diet (HFD) on the remodeling of the lipidome, characterized by a significant increase in longer and more unsaturated acyl chains within the triacylglycerides and phospholipids.

2. RESULTS

2.1. Experimental design, method performance & standardization

Aiming at high reproducibility and standardization of the comprehensive analysis of AT lipids, we focused on developing a shotgun lipidomics method with an expanded dynamic range, high sensitivity, and linearity. The starting material was AT (SAT, GAT and BAT) obtained from mice fed a control (CD) or high-fat diet (HFD). Typically, for preparation of tissue material for lipidomic analysis, samples are homogenized in aqueous buffers. However, following that standard procedure, we faced difficulties pipetting reproducible amounts of homogenized tissue material from the suspensions during aliquoting and dilution steps of the protocol, likely caused by the presence of large amount of fat droplets in homogenized AT samples. This reproducibility issue was solved by homogenization of AT in 50 vol% ethanol and subsequent dilution in pure ethanol (if required).

To determine the optimal sample amount, a range of 35–200 μg of wet weight SAT were extracted in triplicate in the presence of fixed amounts of internal standards, and analzyed by shotgun mass spectrometry. Total lipid content showed a linear response over the indicated range (Figure 1) and was proportional to sample amount, yielding an average of 98 pmol of lipid per μg wet weight. Furthermore, lipid species profiles became independent of sample amount above 70 μg of wet weight (Table S1).

The dynamic range, limit of detection (LOD) and limit of quantification (LOQ) are lipid class-specific parameters, which depend on differential extraction, ionization, and fragmentation efficiencies of the various lipid classes. In order to determine these parameters, lipid class-specific standards were titrated to a fixed amount of AT homogenate. Linearity and proportionality were assessed for 20 lipid classes by linear regression of log-transformed lipid amounts and their intensities, and reported as R^2 and slope, respectively. Both, linearity and proportionality were excellent across a range of up to 4 orders of magnitude for all lipid classes, with values close to 1 for R^2 and slope, respectively (Table 1 & Figure S1). LOD and LOQ were determined by weighted linear regression (with weights being $1/x^2$) based on a signal-to-noise ratio of 3 for LOD and 10 for LOQ. For most lipid classes, LOD is around 1 pmol (Table 1). Provided that an optimal sample amount (100 μg of wet weight) of AT yields ~10,000 pmol of total lipid (Figure 1A), 1 pmol of a given lipid molecule is theoretically detectable in a typical sample, which corresponds to 0.01 mol%.

The reproducibility of the shotgun lipidomics method for AT was assessed by 6 repeated, independent measurements of identical aliquots of AT samples. For the assessment of reproducibility, only lipids present in at least 4 out of 6 replicates were considered. For the 276 lipids that fulfilled this requirement, the relative standard deviation (RSD) of each lipid molecule was calculated and plotted against its

Table 1 — Limit of detection (LOD), Limit of quantification (LOQ), and linearity for various lipid classes in AT.

Class	min (pmol)	LOD (pmol)	LOQ (pmol)	Slope	R^2
CL	0,23	0,83	2,52	0,96	0,99
Cer	0,09	0,67	2,04	0,94	1
ST	1,83	1,71	5,17	1,05	0,9
HexCer	0,09	0,93	2,81	0,94	0,99
LPA	0,09	0,81	2,46	1,04	0,99
LPC	0,23	0,70	2,11	0,97	0,99
LPE	0,09	0,78	2,38	0,94	0,99
LPG	0,09	0,92	2,80	0,94	0,99
LPI	0,09	1,03	3,13	1,01	0,98
LPS	0,09	1,42	4,32	0,99	0,92
SM	0,23	0,95	2,87	0,96	0,99
TAG	1,37	0,66	1,99	0,94	0,99
CE	1,37	3,24	9,83	0,88	0,94
DAG	0,09	0,90	2,72	0,89	0,99
PA	0,27	0,89	2,70	1,23	0,98
PC	0,91	0,92	2,79	0,96	0,99
PE	0,23	1,05	3,18	0,94	0,98
PG	0,09	0,79	2,38	1,03	0,99
PI	0,23	1,17	3,55	0,93	0,98
PS	0,23	1,1	3,32	1,11	0,97

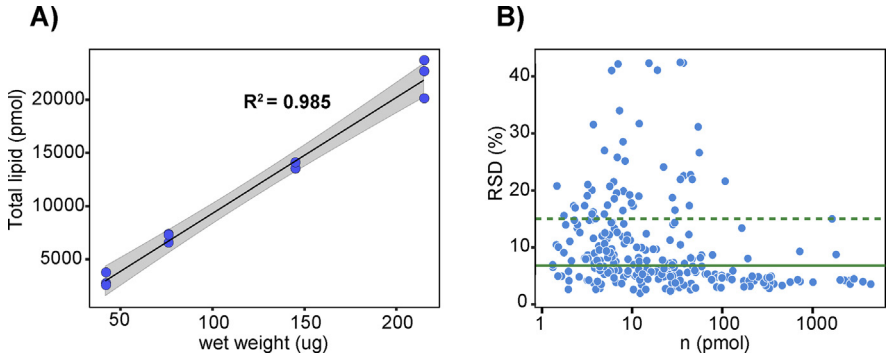

Figure 1: **A)** Linearity and proportionality assessed for total lipid content extracted from various amounts of SAT represented as linear regression of log-transformed lipid amounts and their intensities. **B)** Relative standard deviation (RSD) calculated for 276 lipids present in at least 4 out of 6 replicates. Each lipid molecule RSD was calculated and plotted against its abundance (in pmol). The median technical variation is 6.8% (green solid line) and RSD <15% (green dotted line) was observed for 78.6% of the detected lipids.

abundance (in pmol, Figure 1B) and the data revealed an inverse correlation between lipid abundance and RSD. The median technical variation was 6.8%, while 78.6% of the detected lipids showed an RSD <15%. Taken together, the shotgun lipidomics approach provides a reproducible way to assess lipid abundance in the AT.

2.2. Tissue-specific and diet-related lipidomic trends

Using the newly validated shotgun lipidomics method, WAT (SAT and GAT) and BAT samples obtained from mice fed with either control or high-fat diet were assayed. As expected, the vast majority (~99%) of lipids in all samples were triacylglycerides (TAG). Principal component analysis (PCA) shows that BAT segregates from SAT and GAT along the 1st principal component (PC1) (Figure 2A). This dimension, which explains about 28% of the variance, reveals that groups of samples differ mainly according to tissue type. Interestingly though, upon HFD the BAT lipidome shifts towards a more WAT-like composition, i.e. it approaches that of GAT and SAT samples from HFD-fed mice. In contrast, PC2 mainly explains diet-related differences. While both BAT clusters (CD and HFD) can be clearly distinguished, SAT and GAT samples overlap in the PCA reduced space. We therefore used a different explorative approach called Minimum Curvilinear Embedding (MCE) [27], an unsupervised machine learning for nonlinear dimensionality reduction (Figure 2B). Centered MCE was able to clearly segregate WAT samples on CD and, additionally, uncovered a trend of SAT and GAT samples to separate following HFD, though there was still a partial overlap. These findings are the consequence of a very limited variation between average SAT and GAT lipid species mol% in HFD cohorts, i.e. with a log2 fold change below 1 in almost all species (Table S2). In this experiment the core lipidome of AT, i.e. the species shared by all three tissue types on either diet, consisted of 204 lipids belonging to DAG (6), TAG (195), PC (1), PE (1), ST (1) (Table S3).

PCA and MCE analyses showed that BAT lipidomes are particularly different from SAT and GAT; nevertheless, in all three fat depots TAGs were the major lipid class present, reaching 98–99% of all identified lipids regardless of diet. By excluding TAG lipids from the analysis, we focused on changes concerning the less abundant classes of lipids. Among these, DAGs were the most abundant in WAT (Figure 3), a finding likely associated with lipid metabolism and TAG turnover. In BAT, DAG levels are similar to those of PC and PE and other lipid classes like CL, LPC, PI, and PG that were detected in BAT but remained undetectable in WAT. Importantly, cardiolipins (CL) are present in BAT on both diets, while absent in both SAT and GAT (Figure 3 and Table S4), most likely linked to the larger number of mitochondria in BAT than in WAT [28]. On CD, BAT contains higher amounts of glycerophospholipids and less cholesterol than WAT. However, on HFD, cholesterol tends to increase in BAT while it shows a significant decrease in SAT and GAT.

Following HFD, the acyl chain composition of TAGs (Figure 4A & S2A) in all three AT depots shows a significant decrease of species containing a cumulative 48–50 carbon atoms in their acyl chains, while TAGs with 54–56 carbon atoms increase. Interestingly in BAT as well, TAGs containing 52 carbon atoms decrease significantly, while no substantial changes are observed in SAT or GAT. The increase in length correlates with the increase in the number of double bonds: TAGs containing a total of 0, 1 or 2 double bonds in their acyl chains are more abundant following CD than HFD, where most TAGs contain a total number of 4 and more double bonds. TAGs with 3 double bonds display different trends in brown and white AT. In BAT they significantly increase upon HFD, reaching the average amount displayed by white depots, but they do not change in GAT, whereas in SAT they decrease significantly. In summary, TAGs become longer and more unsaturated when animals are on HFD and these changes are more pronounced in BAT than in WAT.

Remarkably, the changes observed for TAGs are hardly reflected in the acyl chain composition of membrane lipids. Upon HFD, lipids containing 36 carbon atoms significantly increase in abundance, while the abundance of other lipids, both shorter and longer than 36, decreases regardless of the AT depot type (Figure 4B & S2B). The only exception concerns lipids containing 18 carbon atoms: these are lysolipids, and they slightly increase in BAT. The double bond composition displays different trends for white and brown AT, except for monounsaturated lipids, which always decrease on HFD. In white AT, saturated and diunsaturated lipids decrease upon HFD, while in BAT they increase, and lipids containing 3 or 4 double bonds increase, while in BAT they do not change significantly. Polyunsaturated lipids (>4 double bonds) are detected only in BAT, where they significantly decrease on HFD. In

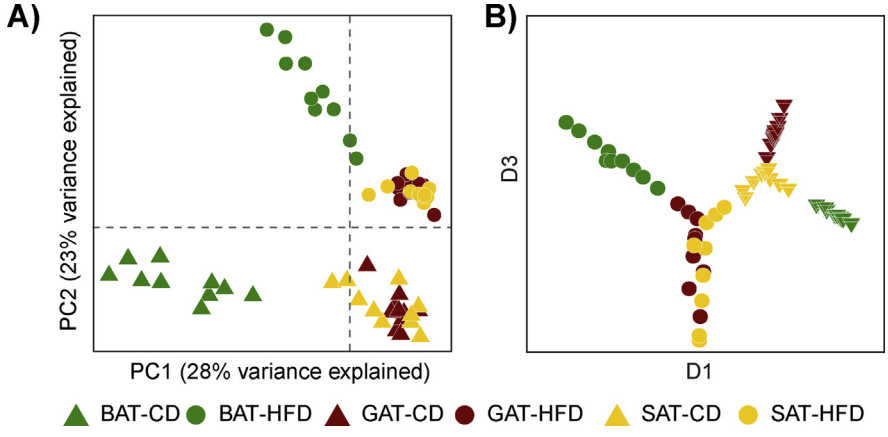

Figure 2: **A**) Principal Component Analysis (PCA) of AT lipidomes. BAT and WAT samples clearly and significantly separate, with GAT and SAT samples from CD-fed mice clustering separately from GAT and SAT samples from HFD-fed mice. PC1 significantly segregates samples according to tissue type, and PC2 significantly segregates samples according to diet. Adjusted p-values (Benjamini-Hochberg correction) for PC1 are: < 0.001 for BAT-CD vs. BAT-HFD; < 0.001 for BAT-CD and BAT-HFD vs. GAT and SAT on CD and HFD; < 0.05 for GAT-CD vs. GAT-HFD and vs. SAT-HFD, and for SAT-CD vs. SAT-HFD; nonsignificant for all other GAT vs. SAT comparisons. Comparisons along PC2 are significant except for GAT vs. SAT on the same diet. **B**) Centered Minimum Curvilinear Embedding (cMCE) on Spearman correlation. Dimensions 1 and 3 significantly differentiate almost all groups of samples. Adjusted p-values (Benjamini-Hochberg correction) for D1 are < 0.001 for all comparisons except for GAT-HFD vs. SAT-HFD where p-value < 0.01, and for GAT-CD vs. SAT-CD where p-value < 0.05. Along D3 all comparisons are significant except GAT-HFD vs. SAT-HFD.

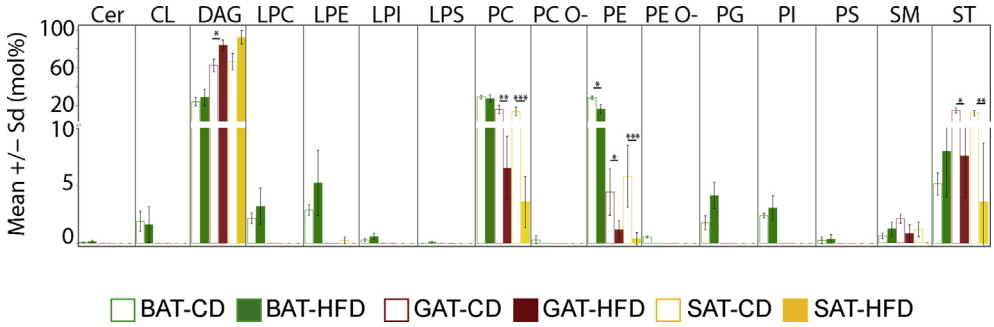

Figure 3: Lipid class composition of white and brown adipose tissues following chow and high-fat diet excluding TAGs. Class abbreviations: Cer — ceramide; CL — cardiolipin; DAG — diacylglyceride; LPC — lysophosphatidylcholine; LPE — lyso-phosphatidylethanolamine; LPI — lysophosphatidylinositol; LPS — lysophosphatidylserine; PC — phosphatidylcholine; PC O- — ether-linked phosphatidylcholine; PE — phosphatidylethanolamine; PE O- — ether-linked phosphatidylethanolamine; PG — phosphatidylglycerol; PI — phosphatidylinositol; PS — phosphatidylserine; SM — sphingomyelin; ST — cholesterol. Asterisks indicate a significant difference between CD and HFD (p-value <0.05*, <0.01**, <0.001***). The different depot types are color coded as follows: BAT green, GAT dark red, SAT yellow. White bars with colored border indicate cohorts on CD, colored bars indicate cohorts on HFD.

WAT depots, the length and unsaturation profiles of membrane lipids and triglycerides follow the same basic rules, as the relative increase in acyl chain length is accompanied by an increase in the number of double bonds. In contrast, in BAT membrane lipids the unsaturation pattern differs from that of triglycerides, in that we observe an inverse behavior of mono- and di-unsaturated species on HFD, and a concomitant clear decrease of highly poly-unsaturated species (mean values and standard deviation of length and unsaturation groups are given in Table S5).

To further understand the diet-dependent changes affecting the lipidome of the various AT depots, we inspected the difference between the means (HFD-CD) of the single subspecies in membrane and storage lipidomes (Figure 5 and S3). By defining a threshold difference of $|0.5|$ mol%, we excluded lipids with a mean mol% < 0.5 in both diets. This highlights the largest differences concerning highly abundant features (i. e. with a mean value on either diet near or above the 75th percentile). The levels of DAGs containing two C18-long acyl chains, e.g. octadecenoic (18:1), octadecadienoic (18:2) and octadecatrienoic (18:3) FA, increase upon HFD in both WAT and BAT, and, simultaneously, DAGs containing either hexadecanoic (16:0) or hexadecenoic (16:1) FA decrease (Figure 5 A—C). A clear exception is DAG 16:0—18:2, which is more abundant in all three AT depots on HFD. It should be noted that in GAT and SAT, lipids with a total length of 36 carbons exclusively belong to the DAGs, whereas in BAT samples, C36 species also occur in other lipid classes (PG, PI, PC). A major difference in the behavior of BAT and WAT during HFD is the abundance of cholesterol. In WAT cholesterol is the major lipid and decreases upon HFD, whereas it accumulates in BAT upon HFD. Interestingly, the lipids that display the highest decrease upon HFD in BAT are three PE species containing eicosatetraenoic acid (16:0/20:4; 18:0/20:4; 18:1/20:4).

The results for TAGs (Figure S3 A—C) support the length and unsaturation profiles shown in Figure 4. Specifically, the greatest differences concern shorter (C50 and C52 total length), less unsaturated subspecies in samples on CD, and longer (C52 and C54), more unsaturated subspecies in samples on HFD. Additional information is given by the acyl chain identified within each TAG: the increased abundance of C54 species in samples on HFD mostly concerns TAGs where the identified acyl chain comprises 18C.

The differences in lipid composition between BAT and WAT are easily distinguished by both PCA and MCE. However, differences between WAT depots are much more difficult to discern, and only MCE succeeded in distinguishing GAT and SAT on both diets, remarkably identifying patterns guided by 'private' features, i.e. lipids exclusive to a given cohort (Table S6). Nonetheless, when focusing on the core lipidome, even MCE cannot segregate GAT and SAT, since abundance patterns are too similar on both diets (Figure S3, Table S3).

3. DISCUSSION

Shotgun lipidomics allows for parallel profiling of hundreds of structurally and functionally diverse lipids. Nevertheless, obtaining a comprehensive, reproducible and quantitative lipidomics analysis of AT is particularly challenging. In addition, AT-specific information on performance of mass spectrometry-based methods is not available [23,26,29,30]. Here, we thoroughly characterized a shotgun lipidomics method for AT analysis and its validation with respect to sample amounts, linearity, sensitivity and reproducibility (Figure 1 & Table 1). This method requires about 100 μg of AT to yield about 10,000 pmol total lipid, which represents an optimal amount for shotgun lipidomics. This is considerably less material than is usually required for the lipidomic analysis of AT which is in the range of several μg of wet weight [30]. It allows the detection of more than 300 individual lipid molecules, belonging to 20 different lipid classes, with a high dynamic range of about 4 orders of magnitude and sensitivity in the sub-μM range, and high reproducibility below 10% RSD. By quantitatively inspecting significant differences between the lipidomes of WAT and BAT from mice fed with control and high-fat diets, we provide proof of concept and validation of the procedure. At the present stage, we cannot provide a mechanistic explanation of the biological processes underlying the observed changes: this requires additional experiments and was beyond the scope of this technical report. We hypothesize that the lipidomic remodeling of AT upon HFD is likely associated with the nature of the fatty acids consumed in the diet and is coupled to the physiological mechanisms by which adipocyte membranes respond to AT expansion, presumably driven by positive energy balance ultimately leading to obesity. In HFD-fed mice, we observed an accumulation of TAGs with a total length of 54 carbons and a concomitant decrease of TAGs with 48—50 carbons (Figure 4A), meaning that 16-carbon acyl chains are replaced by 18-carbon acyl chains (Figure S2). Similarly, we observed an overall accumulation of non-storage lipids made of acyl chains containing 18 carbons and including various numbers of double bonds. In this regard, we noticed a relative increase of DAG, PC and PE species with 18:0, 18:1 and 18:2 acyl chains, alongside a decrease of species containing

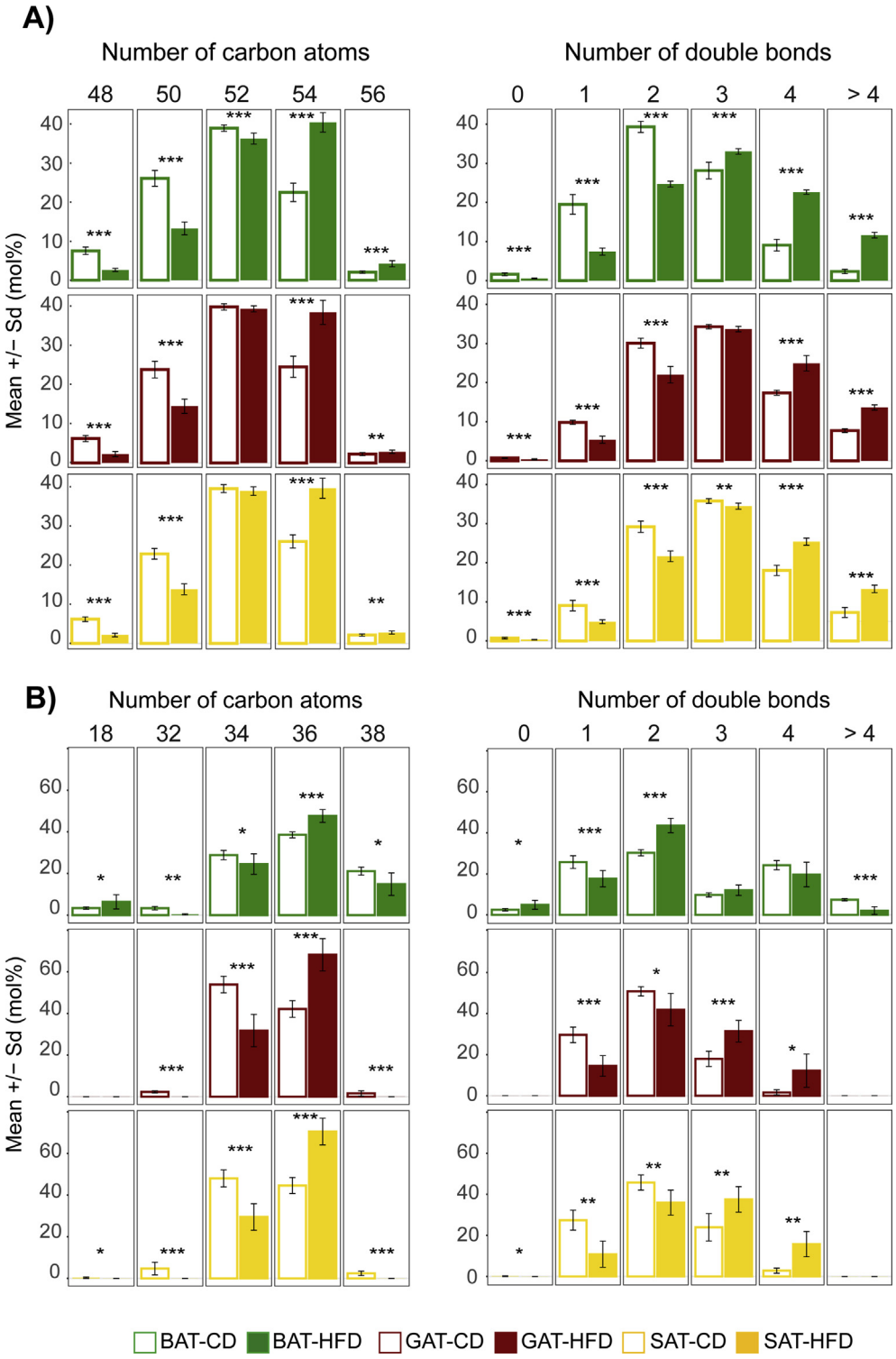

Figure 4: Total acyl chain length (left side) and unsaturation (right side) profiles of: A) TAGs; B) membrane lipids. Lipids were regrouped according to the number of carbon atoms and the number of double bonds present in their acyl chains. Mean and standard deviation were calculated for each cohort using mol% - transformed data. Only length groups >3 mol% are represented; complete acyl chain length profiles of A and B are shown in the Supplementary Figure S3. Asterisks indicate a significant difference between CD and HFD (p-value < 0.05*, <0.01**, <0.001***). The different types of AT are color-coded as follows: BAT green, GAT dark red, SAT yellow. White bars with colored border indicate cohorts on CD; colored bars indicate cohorts on HFD.

the 16-carbon acyl chain (Figure 5). Thus, high fat diet induced an overall increase of longer and more unsaturated triglycerides and phospholipid species in white adipose depots. Although previously published research investigating the lipidomics of AT is not directly comparable to this study, because of the varying experimental settings and techniques adopted to tackle the specific question of each research group, we find a similar trend in a study in human twins discordant for obesity, where results showed that membrane lipids

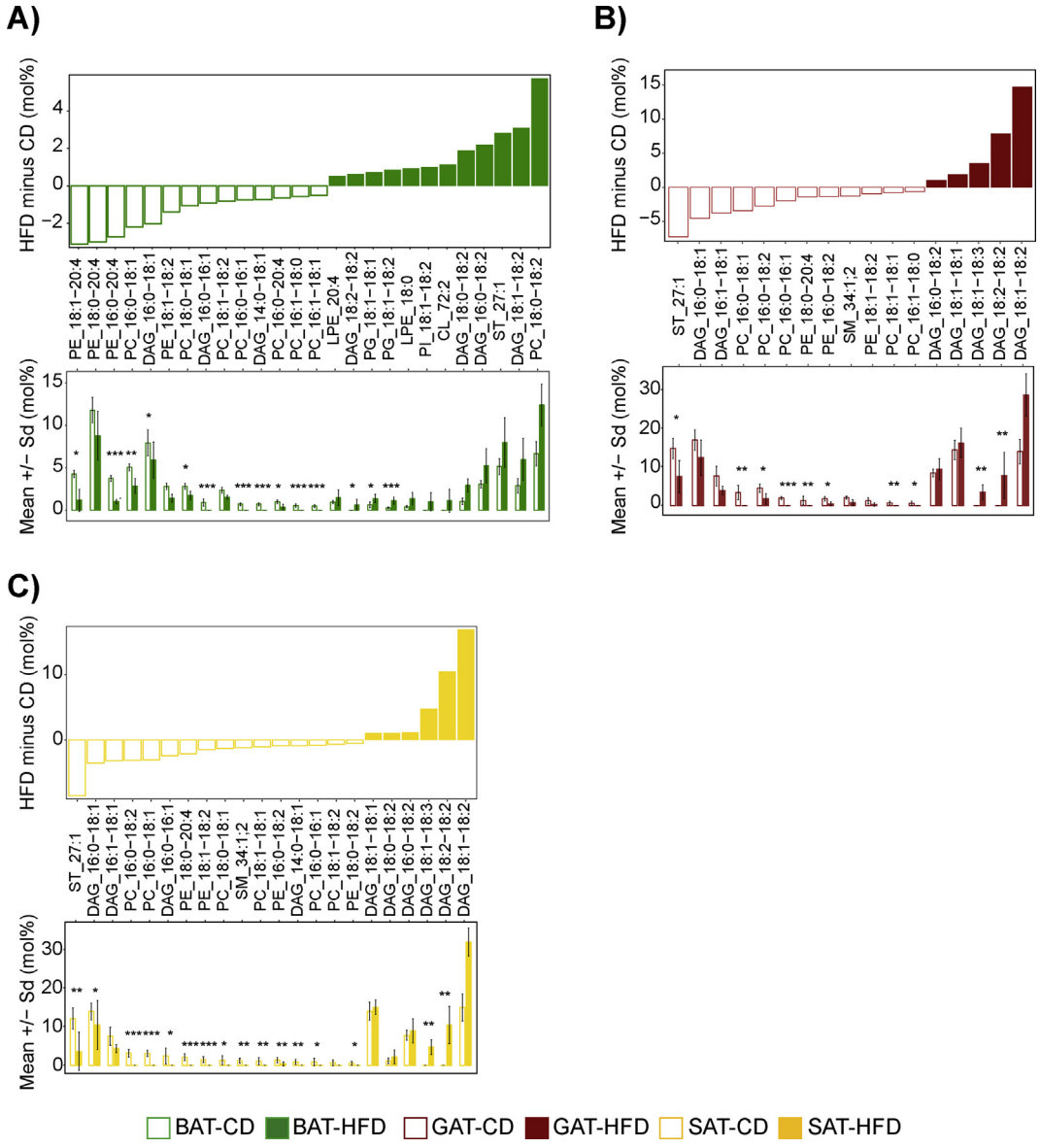

Figure 5: Subspecies level analysis of membrane lipids in fat tissues. Upper panel bar plots represent the difference between the means of HFD and CD in the respective adipose tissues: A) BAT; B) GAT; C) SAT. Only species with $\Delta > |0.5|$ mol% are shown. Lower panel bar plots represent the mean amount and standard deviation of the subspecies in CD and HFD cohorts. Asterisks indicate the species that differ significantly between diets according to the pairwise Mann—Whitney test performed on the log-transformed dataset; p-values were adjusted according to the Benjamini-Hochberg correction for multiple comparisons.

containing longer and more unsaturated fatty acids were more abundant in the obese than in the lean individuals [22].

In comparison to other tissue types the primary function of AT is to accumulate storage lipids. Excess lipids, however, are stored ectopically in other tissues such as muscle, liver, and pancreas, a situation culminating to metabolic dysfunction. Indeed, the expansion of AT in obesity has effects that go beyond body-weight gain, usually associated with increased levels of circulating FAs, and inflammatory mediators that are now recognized as a major cause of decreased insulin sensitivity. Interestingly, many cohort studies reported that some obese individuals display a phenotype referred to as "metabolically healthy obesity," recognized by insulin sensitivity, smaller fat cells, and less pronounced AT inflammation than those observed in insulin-resistant obese individuals [31—33]. It is also established that the two obesity phenotypes differ in SAT gene expression, AMPK activity or oxidative stress [34—36]. Thus, profiling AT lipidomes can advance knowledge of the processes underlying lipid metabolism and resolve differences of AT hypertrophy that correlate with the maintenance of a metabolically healthy status. The protocol presented here precisely provides the platform for addressing this issue.

Some fat depots are implicated more than others in the development of insulin resistance [37,38]. Increasing the number of samples and identifying all three acyl chains of TAGs would shed light on the differences characterizing GAT and SAT, and correlate diet-related lipidomic patterns to metabolic parameters. This would pave the way to a fundamental understanding of the dynamics underlying hypertrophy of distinct WAT depots and the development of metabolic syndrome.

Lipidomics analysis can also supply additional information to studies on the physiology of BAT and the beiging of WAT. In fact, our method could measure the lipidomes of both AT depots from lean and obese individuals, resolving the differences among the tested groups.

Besides generating the distinct profiles of WAT and BAT lipidomes, as previously shown by others [23], the data obtained in this study also provide a snapshot of the diverse response of brown and white AT to overnutrition (Figures 3 & 4). As shown by PCA (Figure 3A), BAT on HFD shifts toward a more WAT-like composition, despite maintaining its identity, since it still clusters separately from WAT samples. BAT's distinct lipidomic profile under HFD is achieved already at class level: its number of lipid classes, higher than that of WAT, remains unchanged on HFD (Figure 3). Additionally, we do not observe any clear change in the total levels of DAGs, a completely different behavior from that exhibited by WAT depots, where DAG levels significantly increase. On the other hand, in all AT on HFD, PE levels significantly drop, while only in BAT cholesterol, PG, PI and SM increase. The similarities of BAT and WAT lipidomes following HFD are visible in the unsaturation and length profiles, where relative amounts of lipids with the same length or number of double bonds converge, independent of their initial differences on CD (Figure 4 & S2). The important and beneficial role of BAT in fatty acid oxidation and thermogenesis has mainly been shown in animal models [26], but recent evidence from human BAT studies was also published [2]. Furthermore, in specific cases human SAT undergoes browning/beiging, associated with an increased whole-body metabolic rate [39]. The interest in increasing BAT metabolism or promoting browning/beiging of WAT in humans as a potential strategy for the treatment of obesity and its related metabolic disorder is enormous. However, investigating the physiological differences of the various AT depots requires a systematic lipidomic analysis as an essential element of the -omics pipeline. This would provide core data towards elucidating AT remodeling mechanisms and thus potentially facilitate the development of therapeutic approaches against obesity-induced metabolic diseases.

The presented method can easily be utilized for non-AT samples containing high amounts of neutral lipids, e.g. tissue samples from subjects with fatty-liver disease [40,41]. Such samples, under common extraction and measurement conditions, would interfere with full lipidomic analysis due to ion suppression. Obtaining detailed lipidomic profiles from patients at various stages of a disease will be crucial for investigating the aetiology of obesity-related pathologies. Samples rich in lipid droplets are another example [42–44]. Studying the biogenesis and metabolism of these organelles or lipid droplet-associated organelles like ER [45] or mitochondria [46] would benefit from monitoring the dynamics of full lipid profiles within the isolated samples. The presented approach offers a solution to handle these challenges.

4. MATERIALS & METHODS

4.1. Chemicals

Water, propan-2-ol, and methanol were purchased from Fischer Scientific. Methyl tert-butyl ether, chloroform, ammonium bicarbonate and ammonium acetate were purchased from Sigma–Aldrich. All chemicals were analytical grade. Synthetic lipid standards were purchased from Avanti Polar Lipids, Larodan Fine Chemicals, and Sigma–Aldrich.

4.2. Feeding of mice

Ten six-week-old female C57BL/6 mice were fed a control diet (CD, D12450B, Research Diets, NJ, USA, 20% protein, 70% carbohydrates, 10% fat), and ten were fed a high fat diet (HFD, D12492, Research Diets, NJ, USA, 20% protein, 20% carbohydrates, 60% fat) for 20 weeks, as previously described [6,10,47]. Experiments were approved by the Landesdirektion Sachsen, Germany.

4.3. Sample preparation

ATs were homogenized directly in a Turrax homogenizer for 60 s in 0.5 ml of ice-cold 150 mM ammonium bicarbonate and ethanol (50/50 v/v). Homogenates were subsequently diluted 1:10 (v/v) in ethanol and used for lipid extraction.

4.4. Lipid extraction

Mass spectrometry-based lipid analysis was performed at Lipotype GmbH (Dresden, Germany) as described [14]. Lipids were extracted using a two-step chloroform/methanol procedure [13]. Samples were spiked with internal lipid standard mixture containing: 30 pmol cardiolipin 16:1/15:0/15:0/15:0 (CL), 30 pmol ceramide 18:1; 2/17:0 (Cer), 100 pmol diacylglycerol 17:0/17:0 (DAG), 30 pmol hexosylceramide 18:1; 2/12:0 (HexCer), 30 pmol lyso-phosphatidate 17:0 (LPA), 50 pmol lyso-phosphatidylcholine 12:0 (LPC), 30 pmol lyso-phosphatidylethanolamine 17:1 (LPE), 30 pmol lyso-phosphatidylglycerol 17:1 (LPG), 20 pmol lyso-phosphatidylinositol 17:1 (LPI), 30 pmol lyso-phosphatidylserine 17:1 (LPS), 50 pmol phosphatidate 17:0/17:0 (PA), 150 pmol phosphatidylcholine 17:0/17:0 (PC), 75 pmol phosphatidylethanolamine 17:0/17:0 (PE), 50 pmol phosphatidylglycerol 17:0/17:0 (PG), 50 pmol phosphatidylinositol 16:0/16:0 (PI), 100 pmol phosphatidylserine 17:0/17:0 (PS), 100 pmol cholesterol ester 20:0 (CE), 50 pmol sphingomyelin 18:1; 2/12:0; 0 (SM), 500 pmol triacylglycerol 17:0/17:0/17:0 (TAG) and 300 pmol cholesterol D6 (Chol). After extraction, the organic phase was transferred to an infusion plate and dried in a speed vacuum concentrator. 1st step dry extract was re-suspended in 7.5 mM ammonium acetate in chloroform/methanol/propanol (1:2:4; V:V:V) and 2nd step dry extract in 33% ethanol solution of methylamine in chloroform/methanol (0.003:5:1; V:V:V). All liquid handling steps were performed using Hamilton Robotics STARlet robotic platform with the Anti Droplet Control feature for organic solvents pipetting.

4.5. Mass spectrometry

Samples were analzyed by direct infusion on a QExactive mass spectrometer (Thermo Scientific) equipped with a TriVersa NanoMate ion source (Advion Biosciences). Samples were analzyed in both positive and negative ion modes with a resolution of $R_{m/z=200} = 280{,}000$ for MS and $R_{m/z=200} = 17{,}500$ for MSMS experiments, in a single acquisition. MSMS was triggered by an inclusion list encompassing corresponding MS mass ranges scanned in 1 Da increments [19]. Both MS and MSMS data were combined to monitor CE, DAG and TAG ions as ammonium adducts; PC, PC O-, as acetate adducts; and CL, PA, PE, PE O-, PG, PI, and PS as deprotonated anions. MS only was used to monitor LPA, LPE, LPE O-, LPI, and LPS as deprotonated anions; Cer, HexCer, SM, LPC, and LPC O- as acetate adduct and cholesterol as ammonium adduct of an acetylated derivative [48].

4.6. Data analysis and post-processing

Data were analzyed with an in-house developed lipid identification software based on LipidXplorer [49,50]. Data post-processing and normalization were performed using an in-house developed data management system. If not stated otherwise, only lipid identification with a signal-to-noise ratio >5, a signal intensity 5-fold higher than in corresponding blank samples, and lipids present in at least 5 out of 10 replicates was considered for further data analysis.

Data were analzyed with R version 3.5 (R Core Team, 2018) using tidyverse packages version 1.1.1 [51] and plots were created with ggplot2 version 2.2.1 [52].

4.7. Lipid nomenclature

When describing different lipid species the following annotations are used: Lipid class-[sum of carbon atoms]:[sum of double bonds]; [sum of hydroxyl groups], i.e. SM-34:1; 2 means an SM species with 34 carbon atoms, 1 double bond and 2 hydroxyl groups in the ceramide backbone. Lipid subspecies annotation contains additional information on the exact identity of their fatty acids. For example, PI-34:1; 0 (18:1; 0—16:0; 0) denotes phosphatidylinositol with a total length of its fatty acids equal to 34 carbon atoms, total number of double bonds in its fatty acids equal to 1 and 0 hydroxylations with C18:1 (oleic) and C16:0 (palmitic) fatty acids. When the exact position of fatty acids in relation to the glycerol backbone (*sn1* or *sn2*) is not discernible a hyphen "-" separating the acyl chains is used. In case the *sn* position is known, acyl chain information is separated by a slash "/". TAG features are reported as pairs of intact ion and neutral loss of a fatty acid. For example, TAG-50:1; 0-FA-18:1; 0 refers to the neutral loss of an 18:1 fatty acid belonging to the intact TAG-50:1; 0 molecule.

4.8. Descriptive statistics of lipidomics data

Lipid features present in less than 50% of the samples in a cohort were filtered in that given cohort. Analyses were performed in R (R Core Team 2018) on the mol%-transformed dataset, i.e., after transforming raw data (picomol) to mole percent (each quantity was divided by the sum of the lipids detected in its respective sample and multiplied by 100). Data structure was analzyed by means of Principal Component Analysis (PCA) using the Singular Value Decomposition function, and by means of the nonlinear machine learning called Minimum Curvilinear Embedding (MCE) [27]. Total carbon chain length and unsaturation plots result from grouping together all the lipids that present the same number of carbon atoms (total length) or the same number of double bonds (unsaturation) and calculating their mean and standard deviation in each cohort of samples. The difference between the means was calculated for each species by subtracting the mean of the controls from the mean of the treated samples (Treated *minus* Reference). Significance was calculated by means of the non-parametric Wilcoxon test and p-values were adjusted after the Benjamini-Hochberg correction. Plots were created with ggplot2 [52].

ACKNOWLEDGMENTS

We thank Cornelia Schroeder and Sider Penkov for critical reading of the manuscript. CK and MAS would like to thank Steffi Lenhard for skillful technical assistance. CK would like to acknowledge stimulating input from Chris Cornell. Funding was provided by Deutsche Forschungsgemeinschaft (DFG, German Research Foundation) — Project Number 288034826 - IRTG 2251 (ÜC), the German Center for Diabetes Research (DZD e.V.) (ÜC) and ERC Consolidator Grant DEMENTIL (683145) (TC).

CONFLICT OF INTEREST

CK is shareholder and employee of Lipotype GmbH. KS is shareholder and CEO of Lipotype GmbH. MAS is a shareholder of Lipotype GmbH and an employee of PORT. This does not alter the authors' adherence to all policies on sharing data and materials.

APPENDIX A. SUPPLEMENTARY DATA

The raw data were deposited on the Mendeley server. The link is https://data.mendeley.com/datasets/kv6bh2zkht/1.

Supplementary data to this article can be found online at https://doi.org/10.1016/j.molmet.2019.01.009.

REFERENCES

[1] Lempradl, A., Pospisilik, J.A., Penninger, J.M., 2015. Exploring the emerging complexity in transcriptional regulation of energy homeostasis. Nature Reviews Genetics 16(11):665—681.

[2] Chondronikola, M., Volpi, E., Borsheim, E., Porter, C., Annamalai, P., Enerback, S., et al., 2014. Brown adipose tissue improves whole-body glucose homeostasis and insulin sensitivity in humans. Diabetes 63(12):4089—4099.

[3] Choe, S.S., Huh, J.Y., Hwang, I.J., Kim, J.I., Kim, J.B., 2016. Adipose tissue remodeling: its role in energy metabolism and metabolic disorders. Frontiers in Endocrinology (Lausanne) 7:30.

[4] Engin, A., 2017. Adipose tissue hypoxia in obesity and its impact on preadipocytes and macrophages: hypoxia hypothesis. Advances in Experimental Medicine & Biology 960:305—326.

[5] Hosogai, N., Fukuhara, A., Oshima, K., Miyata, Y., Tanaka, S., Segawa, K., et al., 2007. Adipose tissue hypoxia in obesity and its impact on adipocytokine dysregulation. Frontiers in Plant Science 56(4):901—911.

[6] Garcia-Martin, R., Alexaki, V.I., Qin, N., Rubin de Celis, M.F., Economopoulou, M., Ziogas, A., et al., 2016. Adipocyte-specific hypoxia-inducible factor 2alpha deficiency exacerbates obesity-induced brown adipose tissue dysfunction and metabolic dysregulation. Molecular and Cellular Biology 36(3):376—393.

[7] Reilly, S.M., Saltiel, A.R., 2017. Adapting to obesity with adipose tissue inflammation. Endocrinology 13(11):633—643.

[8] Hong, C.P., Yun, C.H., Lee, G.W., Park, A., Kim, Y.M., Jang, M.H., 2015. TLR9 regulates adipose tissue inflammation and obesity-related metabolic disorders. Obesity (Silver Spring) 23(11):2199—2206.

[9] Sedger, L.M., Tull, D.L., McConville, M.J., De Souza, D.P., Rupasinghe, T.W., Williams, S.J., et al., 2016. Lipidomic profiling of adipose tissue reveals an inflammatory signature in cancer-related and primary lymphedema. PLoS One 11(5) e0154650.

[10] Chung, K.J., Chatzigeorgiou, A., Economopoulou, M., Garcia-Martin, R., Alexaki, V.I., Mitroulis, I., et al., 2017. A self-sustained loop of inflammation-driven inhibition of beige adipogenesis in obesity. Nature Immunology 18(6):654—664.

[11] Chung, K.J., Nati, M., Chavakis, T., Chatzigeorgiou, A., 2018. Innate immune cells in the adipose tissue. Reviews in Endocrine Metabolic Disorders 19(4):283—292.

[12] Mittendorfer, B., 2011. Origins of metabolic complications in obesity: adipose tissue and free fatty acid trafficking. Current Opinion in Clinical Nutrition and Metabolic Care 14(6):535—541.

[13] Ejsing, C.S., Sampaio, J.L., Surendranath, V., Duchoslav, E., Ekroos, K., Klemm, R.W., et al., 2009. Global analysis of the yeast lipidome by quantitative shotgun mass spectrometry. Proceedings of the National Academy of Science USA 106(7):2136—2141.

[14] Sampaio, J.L., Gerl, M.J., Klose, C., Ejsing, C.S., Beug, H., Simons, K., et al., 2011. Membrane lipidome of an epithelial cell line. Proceedings of the National Acadademy of Science USA 108(5):1903—1907.

[15] Kjellqvist, S., Klose, C., Surma, M.A., Hindy, G., Mollet, I.G., Johansson, A., et al., 2016. Identification of shared and unique serum lipid profiles in diabetes mellitus and myocardial infarction. Journal of American Heart Association 5(12):e004503.

[16] Surma, M.A., Klose, C., Peng, D., Shales, M., Mrejen, C., Stefanko, A., et al., 2013. A lipid E-MAP identifies Ubx2 as a critical regulator of lipid saturation and lipid bilayer stress. Molecular Cell 51(4):519—530.

[17] Mitroulis, I., Ruppova, K., Wang, B., Chen, L.S., Grzybek, M., Grinenko, T., et al., 2018. Modulation of Myelopoiesis Progenitors Is an Integral Component of Trained Immunity. Cell 172(1—2), 147—161 e112.

[18] Stefanko, A., Thiede, C., Ehninger, G., Simons, K., Grzybek, M., 2017. Lipidomic approach for stratification of acute myeloid leukemia patients. PLoS One 12(2) e0168781.

[19] Surma, M.A., Herzog, R., Vasilj, A., Klose, C., Christinat, N., Morin-Rivron, D., et al., 2015. An automated shotgun lipidomics platform for high throughput, comprehensive, and quantitative analysis of blood plasma intact lipids. European Journal of Lipid Science and Technology 117(10):1540–1549.

[20] Carvalho, M., Sampaio, J.L., Palm, W., Brankatschk, M., Eaton, S., Shevchenko, A., 2012. Effects of diet and development on the Drosophila lipidome. Molecular Systems Biology 8:600.

[21] Prasain, J.K., Wilson, L., Hoang, H.D., Moore, R., Miller, M.A., 2015. Comparative lipidomics of caenorhabditis elegans metabolic disease models by SWATH non-targeted tandem mass spectrometry. Metabolites 5(4):677–696.

[22] Pietilainen, K.H., Rog, T., Seppanen-Laakso, T., Virtue, S., Gopalacharyulu, P., Tang, J., et al., 2011. Association of lipidome remodeling in the adipocyte membrane with acquired obesity in humans. PLoS Biology 9(6) e1000623.

[23] May, F.J., Baer, L.A., Lehnig, A.C., So, K., Chen, E.Y., Gao, F., et al., 2017. Lipidomic adaptations in white and brown adipose tissue in response to exercise demonstrate molecular species-specific remodeling. Cell Reports 18(6): 1558–1572.

[24] Baker, R.C., Nikitina, Y., Subauste, A.R., 2014. Analysis of adipose tissue lipid using mass spectrometry. Methods in Enzymology 538:89–105.

[25] Caesar, R., Manieri, M., Kelder, T., Boekschoten, M., Evelo, C., Muller, M., et al., 2010. A combined transcriptomics and lipidomics analysis of subcutaneous, epididymal and mesenteric adipose tissue reveals marked functional differences. PLoS One 5(7):e11525.

[26] Marcher, A.B., Loft, A., Nielsen, R., Vihervaara, T., Madsen, J.G., Sysi-Aho, M., et al., 2015. RNA-Seq and Mass-spectrometry-based lipidomics reveal extensive changes of glycerolipid pathways in brown adipose tissue in response to cold. Cell Reports 13(9):2000–2013.

[27] Cannistraci, C.V., Ravasi, T., Montevecchi, F.M., Ideker, T., Alessio, M., 2010. Nonlinear dimension reduction and clustering by Minimum Curvilinearity unfold neuropathic pain and tissue embryological classes. Bioinformatics 26(18): i531–i539.

[28] Ito, T., Tanuma, Y., Yamada, M., Yamamoto, M., 1991. Morphological studies on brown adipose tissue in the bat and in humans of various ages. Archives of Histology & Cytology 54(1):1–39.

[29] Kotronen, A., Seppanen-Laakso, T., Westerbacka, J., Kiviluoto, T., Arola, J., Ruskeepaa, A.L., et al., 2010. Comparison of lipid and fatty acid composition of the liver, subcutaneous and intra-abdominal adipose tissue, and serum. Obesity (Silver Spring) 18(5):937–944.

[30] Stanley, E.G., Jenkins, B.J., Walker, C.G., Koulman, A., Browning, L., West, A.L., et al., 2017. Lipidomics Profiling of Human Adipose Tissue Identifies a Pattern of Lipids Associated with Fish Oil Supplementation. Journal of Proteome Research 16(9):3168–3179.

[31] Primeau, V., Coderre, L., Karelis, A.D., Brochu, M., Lavoie, M.E., Messier, V., et al., 2011. Characterizing the profile of obese patients who are metabolically healthy. International Journal of Obesity (London) 35(7):971–981.

[32] Sims, E.A., 2001. Are there persons who are obese, but metabolically healthy? Metabolism 50(12):1499–1504.

[33] Samocha-Bonet, D., Chisholm, D.J., Tonks, K., Campbell, L.V., Greenfield, J.R., 2012. Insulin-sensitive obesity in humans - a 'favorable fat' phenotype? Trends in Endocrinology and Metabolism 23(3):116–124.

[34] Xu, X.J., Pories, W.J., Dohm, L.G., Ruderman, N.B., 2013. What distinguishes adipose tissue of severely obese humans who are insulin sensitive and resistant? Current Opinion in Lipidology 24(1):49–56.

[35] Elbein, S.C., Kern, P.A., Rasouli, N., Yao-Borengasser, A., Sharma, N.K., Das, S.K., 2011. Global gene expression profiles of subcutaneous adipose and muscle from glucose-tolerant, insulin-sensitive, and insulin-resistant individuals matched for BMI. Diabetes 60(3):1019–1029.

[36] Qatanani, M., Tan, Y., Dobrin, R., Greenawalt, D.M., Hu, G., Zhao, W., et al., 2013. Inverse regulation of inflammation and mitochondrial function in adipose tissue defines extreme insulin sensitivity in morbidly obese patients. Diabetes 62(3):855–863.

[37] Sethi, J.K., Vidal-Puig, A.J., 2007. Thematic review series: adipocyte biology. Adipose tissue function and plasticity orchestrate nutritional adaptation. Journal of Lipid Research 48(6):1253–1262.

[38] Wajchenberg, B.L., Giannella-Neto, D., da Silva, M.E., Santos, R.F., 2002. Depot-specific hormonal characteristics of subcutaneous and visceral adipose tissue and their relation to the metabolic syndrome. Hormone and Metabolic Research 34(11-12):616–621.

[39] Sidossis, L.S., Porter, C., Saraf, M.K., Borsheim, E., Radhakrishnan, R.S., Chao, T., et al., 2015. Browning of Subcutaneous white adipose tissue in humans after severe adrenergic stress. Cell Metabolism 22(2):219–227.

[40] Feng, S., Gan, L., Yang, C.S., Liu, A.B., Lu, W., Shao, P., et al., 2018. Effects of stigmasterol and beta-sitosterol on nonalcoholic fatty liver disease in a mouse model: a lipidomic analysis. Journal of Agricultural and Food Chemistry 66(13): 3417–3425.

[41] Puri, P., Baillie, R.A., Wiest, M.M., Mirshahi, F., Choudhury, J., Cheung, O., et al., 2007. A lipidomic analysis of nonalcoholic fatty liver disease. Hepatology 46(4):1081–1090.

[42] Hartler, J., Kofeler, H.C., Trotzmuller, M., Thallinger, G.G., Spener, F., 2014. Assessment of lipidomic species in hepatocyte lipid droplets from stressed mouse models. Scientific Data 1:140051.

[43] Chitraju, C., Trotzmuller, M., Hartler, J., Wolinski, H., Thallinger, G.G., Lass, A., et al., 2012. Lipidomic analysis of lipid droplets from murine hepatocytes reveals distinct signatures for nutritional stress. Journal of Lipid Research 53(10):2141–2152.

[44] Zhi, Y., Taylor, M.C., Campbell, P.M., Warden, A.C., Shrestha, P., El Tahchy, A., et al., 2017. Comparative lipidomics and proteomics of lipid droplets in the mesocarp and seed tissues of chinese tallow (Triadica sebifera). Frontiers in Plant Science 8:1339.

[45] Markgraf, D.F., Klemm, R.W., Junker, M., Hannibal-Bach, H.K., Ejsing, C.S., Rapoport, T.A., 2014. An ER protein functionally couples neutral lipid metabolism on lipid droplets to membrane lipid synthesis in the ER. Cell Reports 6(1):44–55.

[46] Benador, I.Y., Veliova, M., Mahdaviani, K., Petcherski, A., Wikstrom, J.D., Assali, E.A., et al., 2018. Mitochondria Bound to Lipid Droplets Have Unique Bioenergetics, Composition, and Dynamics that Support Lipid Droplet Expansion. Cell Metabolism 27(4), 869–885 e866.

[47] Chatzigeorgiou, A., Chung, K.J., Garcia-Martin, R., Alexaki, V.I., Klotzsche-von Ameln, A., Phieler, J., et al., 2014. Dual role of B7 costimulation in obesity-related nonalcoholic steatohepatitis and metabolic dysregulation. Hepatology 60(4):1196–1210.

[48] Liebisch, G., Binder, M., Schifferer, R., Langmann, T., Schulz, B., Schmitz, G., 2006. High throughput quantification of cholesterol and cholesteryl ester by electrospray ionization tandem mass spectrometry (ESI-MS/MS). Biochimica et Biophysica Acta 1761(1):121–128.

[49] Herzog, R., Schuhmann, K., Schwudke, D., Sampaio, J.L., Bornstein, S.R., Schroeder, M., et al., 2012. LipidXplorer: a software for consensual cross-platform lipidomics. PLoS One 7(1) e29851.

[50] Herzog, R., Schwudke, D., Schuhmann, K., Sampaio, J.L., Bornstein, S.R., Schroeder, M., et al., 2011. A novel informatics concept for high-throughput shotgun lipidomics based on the molecular fragmentation query language. Genome Biology 12(1):R8.

[51] Wickham, H., 2017. tidyverse: Easily Install and Load the 'Tidyverse'. R package version 1.1.1.

[52] Wickham, H., 2009. ggplot2: elegant graphics for data analysis. New York: Springer-Verlag.

